Direct Solution of 2D Heat Transfer Problems in Frequency Domain with Dynamic Boundary Conditions

R. ZHANG[1], C. ZHANG[2] AND J. JIANG[3]
[1, 2]Department of Mechanical and Materials Engineering
[3]Department of Electrical and Computer Engineering
The University of Western Ontario
London, Ontario N6A 5B9
CANADA

Abstract: - To design a good control system, it is essential to have accurate dynamic models of the system being controlled. Frequency response techniques can be used to develop such dynamic models. In this paper, a new approach for direct solution of the frequency response of 2D heat transfer problems with nonlinear source terms and dynamic boundary conditions is proposed. Three typical boundary conditions are used in the frequency domain. A nonlinear source term due to radiation is employed to determine whether the new approach can be applied to nonlinear systems. Using the frequency response of the system, the transfer function of the linearized system can be obtained subsequently. The performance of the proposed approach has been validated against the results obtained from full-scale computational fluid dynamics (CFD) simulation and excellent agreement has been obtained.

Key Words: - Dynamic model, Frequency response, Transfer function, Numerical simulation, Heat transfer

1 Introduction

The idea of frequency response was proposed by Fourier over 200 years ago. It was then further developed by Nyquist [1] in 1930's. The frequency response technique is widely used in the control engineering to describe the dynamic properties of systems and in aid of control system designs. Even though frequency response techniques have been extended to nonlinear systems through so-called Describing Functions, it is mainly applicable for linear systems. Therefore, in many industry applications, nonlinear dynamic systems are often linearized first so that their dynamic behaviours can be described in terms of frequency responses and the available linear control system design techniques can be applied for controller synthesis. The linearization is normally under the condition that the amplitude of the input signal around a certain steady-state condition is small enough so that the nonlinear aspects of the system can be reasonably approximated [2]. In a stable linearized system, if a low amplitude sinusoidal signal is applied to its input, all related system variables will also be in the form of sinusoidal signals of the same frequency at the steady state. Choosing a variable as the reference, the rest of the system variables can be represented in terms of changes in gains and phase shifts with respect to the reference. If a sequence of sinusoidal signals at different frequencies is applied, the relative gains and phase shifts at the applied frequencies will constitute the frequency response [3].

The frequency response can be determined by experiments if the physical system is available. Alternatively, one can also solve the underlying governing partial differential equations using computational fluid dynamics (CFD) method with sinusoidal inputs at different frequencies to obtain the frequency response [4, 5, 6, 7]. In the CFD approach, the frequency response of a system could be acquired by solving the unsteady governing equations for input signals at different frequencies when all the transients die out.

The frequency response of an industrial furnace was developed by Jiang *et al*. [6, 7] using the CFD approach. When the furnace inputs consist of low amplitude sinusoidal signals around the steady-state condition, the furnace outputs demonstrate dominant sinusoidal signals of the same frequency. Based on this approach, a PID controller has been designed to control this furnace. Although this is a successful application of CFD approach to determine the dynamic behaviour of a complex system, such an approach has several limitations: (1) the accumulated errors due to the discrete time steps in CFD will affect the accuracy of the phase shift, and (2) to determine the gain and phase shift at each frequency, it requires at least twenty time steps in the CFD simulation. This is extremely time-consuming in

particular at low frequencies. Realizing the drawbacks of this CFD approach, a new method was proposed by Zhang *et al*. [8] to obtain the frequency response directly from the partial differential equation in the frequency domain, which is derived from the governing partial differential equation in time domain. Therefore, the error comes only from the grid size used to discretize the partial differential equation in the frequency domain. The computational complexity is in the same order as that for solving a steady-state problem. However, previous work [8] is only applicable to a system with a dynamic temperature boundary condition. This current work extends previous work [8] to more general cases. In this study, three types of heat transfer boundary conditions are considered. A 2D heat transfer problem is employed to demonstrate its capability to solve the heat transfer problem with different types of boundary conditions.

2 Heat Transfer Equation and Boundary Conditions in the Frequency Domain

In this study, a 2D conduction heat transfer problem is used to demonstrate the proposed approach. The geometry of the 2D heat transfer problem as shown in Fig. 1 has unit depth on the *z*-direction. The radiation as a source term is applied on the two surfaces in the *z*-direction, as shown in Fig. 1.

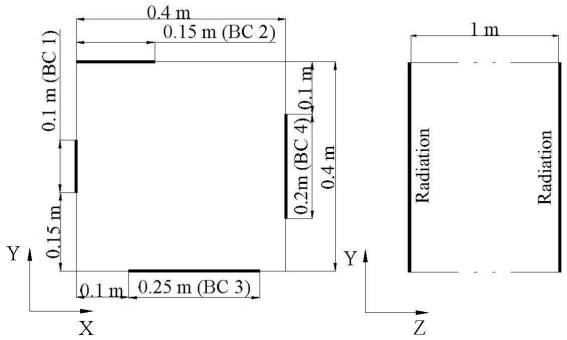

Fig. 1 Geometry of the 2D heat transfer problem

The governing equation for 2D transient conduction heat transfer in the time domain is [9]:

$$\rho c_p \frac{\partial \theta}{\partial t} = k\frac{\partial^2 \theta}{\partial x^2} + k\frac{\partial^2 \theta}{\partial y^2} + S_p \tag{1}$$

where θ is the temperature and S_p is the source term due to radiation heat transfer and can be expressed as:

$$S_p = \varepsilon\sigma A\left(\theta_\infty^4 - \theta^4\right) \tag{2}$$

where θ_∞ is the ambient temperature.

Three types of heat transfer boundary conditions are considered. They are Dirichlet boundary condition (fixed temperature), Neumann boundary condition (fixed heat flux), and Robin boundary condition (convective). The boundary conditions for this 2D conduction heat transfer problem under steady-state condition, which are called the steady boundary conditions, are specified as fixed temperature on *BC1*, fixed heat flux on *BC2*, convective heat transfer on *BC3*, fixed temperature on *BC4*, and insulated condition on the rest of the boundaries for the 2D domain as shown in Fig. 1.

2.1 Heat transfer equation in the frequency domain

The 2D conduction heat transfer equation in the frequency domain can be derived based on the equation in the time domain, i.e., Eq. (1). Under the linear assumption, the sinusoidal temperature signal can be expressed by:

$$\tilde{\theta}(x,y,t) = \theta_m(x,y)\sin\left[\omega t + \varphi(x,y)\right] \tag{3}$$

where the angular frequency ω of the input signal, the period T and the frequency f have a relation of $\omega = \frac{2\pi}{T} = 2\pi f$. The solution will consist of two terms: transient and steady state solutions:

$$\begin{aligned}\theta(x,y,t) &= \theta_0(x,y) + \tilde{\theta}(x,y,t)\\ &= \theta_0(x,y) + \theta_m(x,y)\sin\left[\omega t + \varphi(x,y)\right]\end{aligned} \tag{4}$$

The nonlinear source term, S_p, in Eq. (1) can be linearized as

$$S_p = Q + R*\theta(x,y,t) \tag{5}$$

where $Q = \varepsilon\sigma A\left[\theta_\infty^4 - \theta_0^4(x,y)\right]$; $R = -2\varepsilon\sigma A\,\theta_0^3(x,y)$.

In Eq. (5), the higher order terms of sinusoidal signals are neglected due to the linear assumption. Substituting Eq. (4) into Eq. (1) and subtracting the steady-state governing equation from Eq. (1), the following equation can be obtained

$$\begin{aligned}&\rho c_p \omega\theta_m \cos(\omega t+\varphi)\\ &= k\begin{bmatrix}\theta_{m,xx}\sin(\omega t+\varphi) + \theta_{m,yy}\sin(\omega t+\varphi)\\ -\theta_m\varphi_{,x}^2\sin(\omega t+\varphi) - \theta_m\varphi_{,y}^2\sin(\omega t+\varphi)\\ +\theta_m\varphi_{,xx}\cos(\omega t+\varphi) + \theta_m\varphi_{,yy}\cos(\omega t+\varphi)\\ +2\theta_{m,x}\varphi_{,x}\cos(\omega t+\varphi)\\ +2\theta_{m,y}\varphi_{,y}\cos(\omega t+\varphi)\end{bmatrix}\\ &+ R\theta_m\sin(\omega t+\varphi)\end{aligned} \tag{6}$$

Since Eq. (6) is valid for any instant time, let's select 2 specific values of t, so that

$$\omega t+\varphi=2k\pi,\ \omega t+\varphi=2k\pi+\frac{\pi}{2},\ k=1,2,3...$$

Substituting these two values into Eq. (6), it follows:

$$k\left(\theta_{m,xx}+\theta_{m,yy}\right)+\left[R-k\left(\varphi_{,x}^2+\varphi_{,y}^2\right)\right]\theta_m=0 \tag{7a}$$

$$\begin{aligned}&k\left(\theta_m\varphi_{,xx}+\theta_m\varphi_{,yy}+2\theta_{m,x}\varphi_{,x}+2\theta_{m,y}\varphi_{,y}\right)\\&-\rho c_p\omega\theta_m=0\end{aligned} \tag{7b}$$

Equations (7a) and (7b) are two independent equations with 2 unknowns, amplitude θ_m and phase shift φ.

2.2 Boundary conditions in the frequency domain

To solve the heat transfer equation in the frequency domain for sinusoidal signal inputs, it is necessary to derive the dynamic boundary conditions in the frequency domain.

Dirichlet boundary condition

When the Dirichlet boundary condition is used as the dynamic boundary condition, the amplitude of the dynamic temperature is set at the desired value and the phase shift is set to 0 at the boundary nodes. This will be the reference phase for all other variables. If the desired amplitude of the temperature on the boundary is represented as θ_B, the corresponding boundary condition can be expressed as:

$$\theta_{m,BND}=\theta_B;\ \varphi_{BND}=0 \tag{8}$$

where *BND* is the node on the boundary and *P* is the interior node adjacent to the boundary node. Their locations are illustrated in Fig. 2.

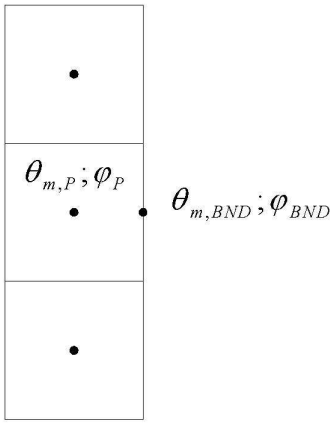

Fig. 2 Locations of node *BND* and node *P*

When the Dirichlet boundary condition is used only as a steady boundary condition, there will be no dynamic signal on the boundary nodes and the boundary condition will become:

$$\theta_{m,BND}=0;\ \varphi_{BND}=\varphi_P \tag{9}$$

By setting φ_{BND} equal to φ_P, one will be able to ensure the continuity of the phase shift at the boundary. The heat flux can be calculated using

$$q_m\sin\left(\omega t+\varphi_q\right)=-\sum^{boundary}\frac{kA}{\Delta x}\theta_{m,P}\sin\left(\omega t+\varphi_P\right) \tag{10}$$

where q_m and φ_q are the amplitude and the phase shift of the dynamic heat flux respectively. This is a vector summation of all the heat flux through the boundary nodes.

Neumann boundary condition

For the Neumann boundary condition, the heat flux is specified on the boundary node *BND*. When it is treated as a dynamic boundary condition, the heat flux can be expressed as:

$$\dot{q}(t)=\dot{q}_B\sin(\omega t)=k\left[\begin{array}{c}\theta_{m,x}\sin(\omega t+\varphi)\\+\theta_m\varphi_{,x}\cos(\omega t+\varphi)\end{array}\right]_{BND} \tag{11}$$

The amplitude of the dynamic heat flux is assumed to be $\dot{q}_B$, and the phase shift of the heat flux is set to 0 and used as the reference to all other variables. Because the heat flux is a derivative of the temperature on the boundary nodes, the temperatures on the boundary nodes need to be updated in each iteration. To obtain the amplitude of the dynamic temperature on the boundary node $\theta_{BND,m}$, one can set $\omega t=\pi/2$. Subsequently, Eq. (11) becomes:

$$\dot{q}_B=k\left[\begin{array}{c}\theta_{m,BND,x}\sin\left(\frac{\pi}{2}+\varphi_{BND}\right)\\+\theta_{m,BND}\varphi_{BND,x}\cos\left(\frac{\pi}{2}+\varphi_{BND}\right)\end{array}\right] \tag{12}$$

For small φ_{BND}, $\cos(\pi/2+\varphi_{END})\approx 0$, which leads to $\dot{q}_B\approx k\theta_{m,BND,x}$. Therefore, $\theta_{BND,m}$ can be approximated by:

$$\theta_{m,BND}=\theta_{m,p}+\dot{q}_B\,\Delta x/k \tag{13}$$

To determine the phase shift on the boundary node, one can set $\omega t=-\varphi_{BND}$,

$$\dot{q}_B\sin\left(-\varphi_{BND}\right)=k\theta_{m,BND}\varphi_{BND,x} \tag{14}$$

where φ_{BND} is given by:

$$\varphi_{BND} = \varphi_p + \dot{q}_B \Delta x \sin(-\varphi_{BND})/k\theta_{BND} \quad (15)$$

If the heat flux is used as the steady boundary condition, the dynamic heat flux is set to 0, the boundary condition becomes an insulated condition in the frequency domain, and the boundary condition is given by:

$$\theta_{m,BND} = \theta_{m,P}; \varphi_{BND} = \varphi_P \quad (16)$$

Robin boundary condition

When the Robin heat transfer boundary condition is used as a dynamic boundary condition, the convective heat transfer coefficient h and ambient temperature θ_∞ will contain dynamic signals. They can be expressed as

$$h(t) = h_0 + h_m \sin(\omega t) \quad (17)$$

$$\theta_\infty(t) = \theta_0 + \theta_{m,\infty} \sin(\omega t) \quad (18)$$

where $h(t)$ is the instantaneous heat transfer coefficient and it is the sum of h_0, the heat transfer coefficient under steady condition, and $\tilde{h}(t)$, the dynamic heat transfer coefficient. Similarly, $\theta_\infty(t)$, θ_0 and $\tilde{\theta}(t)$ are the instantaneous, steady state and dynamic ambient temperatures, respectively.

When the heat transfer coefficient contains a dynamic signal and the ambient temperature is at its steady value, the dynamic energy conservation for the node *P* can be shown as:

$$\int_{t_1}^{t_2} \rho c_p V_P d\theta_P(t) = \int_{t_1}^{t_2} k \sum_{i=1}^{n} A_i \frac{\partial \tilde{\theta}}{\partial x_i} dt - \int_{t_1}^{t_2} A_{BND}\left[h_0 \tilde{\theta}_{BND} + \tilde{h}(\theta_{0,BND} - \theta_\infty)\right] dt \quad (19)$$

where the subscript *i* denotes the interior nodes adjacent to the node *P*. The term on the left hand side of Eq. (19) is the change in the internal energy in the volume surrounding the node *P* from time t_1 to time t_2 This internal energy change is due to the conductive heat flux from the adjacent interior nodes, which is the first term on the right hand of Eq. (19), and the convective heat flux from the boundary, which is the second term on the right hand of Eq. (19). The system has been simplified to a linear system after the higher order term in the convective heat flux is neglected.

To determine the amplitude of the dynamic temperature, one can integrate Eq. (19) and select two specific time, t_1 and t_2, to ensure

$\omega t_1 + \varphi_P = 2k\pi$, $\omega t_2 + \varphi_P = 2k\pi + \frac{\pi}{2}$, $k = 0,1,2$

Letting $\Delta\varphi_i = \varphi_i - \varphi_P$, $\Delta\varphi_{BND} = \varphi_{BND} - \varphi_P$, $\Delta\varphi_h = \varphi_h - \varphi_P$, we have:

$$\begin{aligned} &\rho c_p V_P \theta_{m,P} \\ &= -\frac{k}{\omega} \sum_{i=1}^{n} \frac{A_i}{\Delta x_i} \left\{ \theta_{m,i} \left[\cos\left(\frac{\pi}{2} + \Delta\varphi_i\right) - \cos(\Delta\varphi_i) \right] + \theta_{m,P} \right\} \\ &+ \frac{A_{BND}}{\omega} \left\{ \begin{array}{l} h_0 \theta_{m,BND} \left[\cos\left(\frac{\pi}{2} + \Delta\varphi_{BND}\right) - \cos(\Delta\varphi_{BND}) \right] \\ + h_m(\theta_{0,BND} - \theta_\infty) \left[\cos\left(\frac{\pi}{2} + \Delta\varphi_h\right) - \cos(\Delta\varphi_h) \right] \end{array} \right\} \end{aligned} \quad (20)$$

Equation (20) is the energy balance for the node *P* in one fourth of a period. Then, the amplitude of the dynamic temperature on the boundary node can be expressed as:

$$\theta_{m,BND} = \frac{\left\{ \begin{array}{l} \omega \rho c_p V_P \theta_{m,P} + k \sum_{i=1}^{n} \frac{A_i}{\Delta x_i} * \\ \left\{ \theta_{m,i} \left[\cos\left(\frac{\pi}{2} + \Delta\varphi_i\right) - \cos(\Delta\varphi_i) \right] + \theta_{m,P} \right\} \\ - A_{BND} h_m (\theta_{0,BND} - \theta_\infty) \left[\cos\left(\frac{\pi}{2} + \Delta\varphi_h\right) - \cos(\Delta\varphi_h) \right] \end{array} \right\}}{A_{BND} h_0 \left[\cos\left(\frac{\pi}{2} + \Delta\varphi_{BND}\right) - \cos(\Delta\varphi_{BND}) \right]} \quad (21)$$

Then taking the time derivative for Eq. (19), and setting a specific value for *t* to ensure

$\omega t + \varphi_P = 2k\pi, \quad k = 0,1,2...$

The phase shift on the boundary node *BND* can be derived as:

$$\sin(\Delta\varphi_{BND}) = \frac{\left[\begin{array}{l} k \sum_{i=1}^{n} A_i \frac{\theta_{m,i} \sin(\Delta\varphi_i)}{\Delta x_i} \\ - \omega \rho c_p V_P \theta_{m,P} \\ - A_{BND} h_m (\theta_{0,BND} - \theta_\infty) \sin(\Delta\varphi_h) \end{array} \right]}{A_{BND} h_0 \theta_m} \quad (22)$$

$$\varphi_{BND} = \varphi_P + \Delta\varphi_{BND} \quad (23)$$

Equations (21) - (23) are expressions for the boundary condition when the convective heat transfer coefficient contains a dynamic signal. Similarly, the expression of the boundary condition when the ambient temperature contains a dynamic signal can be expressed as:

$$\theta_{m,BND}=\frac{\left\{\begin{array}{l}\omega\rho c_p V_P\theta_{m,P}+k\sum_{i=1}^{n}\frac{A_i}{\Delta x_i}*\\ \left\{\theta_{m,i}\left[\cos\left(\frac{\pi}{2}+\Delta\varphi_i\right)-\cos\left(\Delta\varphi_i\right)\right]+\theta_{m,P}\right\}\\ +A_{BND}h_0\theta_{\infty,m}\left[\begin{array}{l}\cos\left(\frac{\pi}{2}+\Delta\varphi_\infty\right)\\ -\cos\left(\Delta\varphi_\infty\right)\end{array}\right]\end{array}\right\}}{A_{BND}h_0\left[\cos\left(\frac{\pi}{2}+\Delta\varphi_{BND}\right)-\cos\left(\Delta\varphi_{BND}\right)\right]} \quad (24)$$

$$\sin(\Delta\varphi_{BND})=\frac{\left[\begin{array}{l}k\sum_{i=1}^{n}A_i\frac{\theta_{m,i}\sin\left(\Delta\varphi_i\right)}{\Delta x_i}\\ +A_{BND}h_0\theta_{m,\infty}\sin\left(\Delta\varphi_\infty\right)\\ -\omega\rho c_p V_P\theta_{m,P}\end{array}\right]}{A_{BND}h_0\theta_{m,BND}} \quad (25)$$

$$\varphi_{BND}=\varphi_P+\Delta\varphi_{BND} \quad (26)$$

When a convective heat transfer is used as a steady boundary condition, the boundary condition in the frequency domain becomes:

$$\theta_{m,BND}=\frac{\frac{k}{\Delta x}\sin\left(\omega t+\varphi_P\right)\theta_{m,P}}{h+\frac{k}{\Delta x}\sin\left(\omega t+\varphi_P\right)} \quad (27)$$

$$\varphi_{BND}=\varphi_P \quad (28)$$

3 Comparison of the Frequency Response by the Direct Solution and Full-Scale CFD Approach

The material of the 2D conduction heat transfer problem shown in Fig. 1 is aluminum with constant properties of $k=202.4\,W/mK$, $\rho=2719\ kg/m^3$ and $c_p=871\,kJ/kgK$. First, the temperature distribution is obtained under the steady-state condition. Then, the dynamic signals at different frequencies are applied to different boundaries to obtain the frequency responses. The steady-state boundary conditions are set as: BC1 has a fixed temperature of $\theta_{BC1}=1100K$, BC2 has a fixed heat flux of $Q_{BC2}=-2*10^5\,W/m^2$, BC3 is subject to a convective heat transfer condition with the ambient temperature of $\theta_{\infty,BC3}=250K$ and heat transfer coefficient of $h_{BC3}=200W/m^2K$, BC4 has a fixed temperature of $\theta_{BC4}=500K$, and the ambient temperature is $\theta_\infty=200K$. In the frequency response calculations, the dynamic signals with amplitude of 10% of its steady-state value are applied to the different boundaries to ensure the linear assumption. There are four dynamic signals:

(1) The dynamic temperature on the boundary BC1
$\tilde{\theta}=0.1*\theta_{BC1}*\sin\left(\omega t\right)=110*\sin\left(\omega t\right)\ [K]$
(2) The dynamic heat flux on BC2
$\tilde{Q}_{BC2}=0.1Q_{BC2}\sin(\omega t)=-2\cdot10^4\sin(\omega t)\ [W/m^2]$,
(3) The dynamic heat transfer coefficient on BC3
$\tilde{h}_{BC3}=0.1h_{BC3}\sin(\omega t)=20\sin(\omega t)\ [W/m^2K]$
(4) The dynamic ambient temperature on BC3
$\tilde{\theta}_{\infty,BC3}=0.1\theta_{\infty,BC3}\sin(\omega t)=25\sin(\omega t)\ [W/m^2K]$.

In this study, the dynamic signals are applied only to one boundary at a time and the steady-state boundary conditions are applied to the rest of the boundaries. The frequency of the dynamic signals starts from $\omega_1=1e-4\ rad/\sec$, and increases by $\omega_n=\omega_{n-1}*10^{0.25}\ rad/\sec\ (n=2,3...)$. Dynamic heat flux on BC4 is recorded.

For comparison purpose, the transient heat transfer process due to dynamic boundary conditions is also solved by the full-scale CFD approach using a commercial package, FLUENT. The variation of the dynamic heat flux on BC4 when the dynamic temperature $\tilde{\theta}=110*\sin\left(0.00316*t\right)\ K$ is applied on BC1 is shown in Fig. 3. It can be seen that the dynamic gain ($\tilde{Q}_{BC4}$) and phase shift (φ_{BC4}) are clearly shown. While, it is also found that the amplitude of the signals becomes very low at high frequency. Therefore, there is an upper limit when using CFD approaches to obtain frequency response. In this case, the upper limit is about $\omega=0.0178\ rad/\sec$. On the other hand, the proposed approach is analytical in nature and it does not suffer from this limitation. Figures 4 and 5 illustrate the results using the proposed approach. The figures show the distributions of the gain and phase shift for the local dynamic temperature when a dynamic temperature is applied to BC1 with medium

and high frequencies of $\tilde{\theta} = 110 * \sin(0.00316 * t)\ K$ and $\tilde{\theta} = 110 * \sin(0.562 * t)\ K$, respectively. It can be seen that at the medium frequency (Fig. 4), the spatial distributions of the gain and phase shift are smoother as compared with the case at the high frequency (Fig. 5).

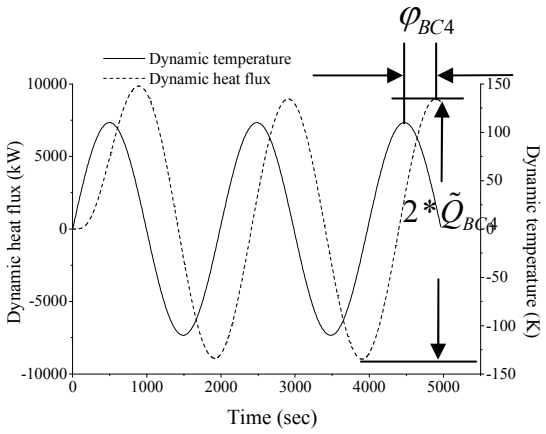

Fig. 3 Dynamic heat flux on BC4 with the dynamic temperature

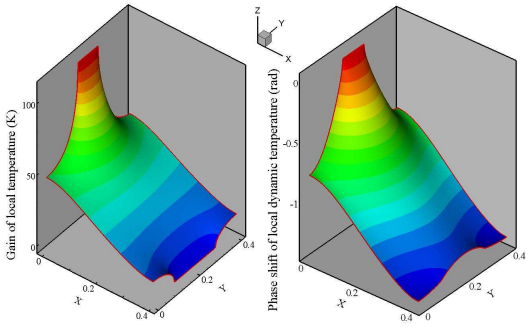

Fig. 4 Gain and the phase shift of the dynamic temperature distribution with dynamic temperature $\tilde{\theta} = 110 * \sin(0.00316 * t)\ K$ on BC1

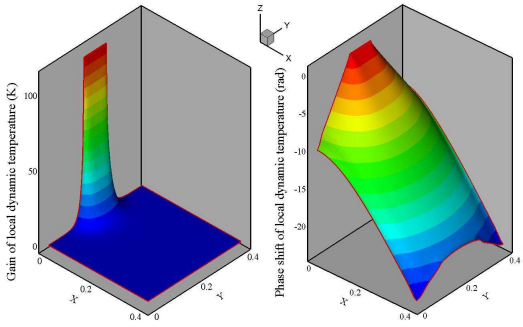

Fig. 5 Gain and the phase shift of the dynamic temperature distribution with dynamic temperature $\tilde{\theta} = 110 * \sin(0.562 * t)\ K$ on BC1

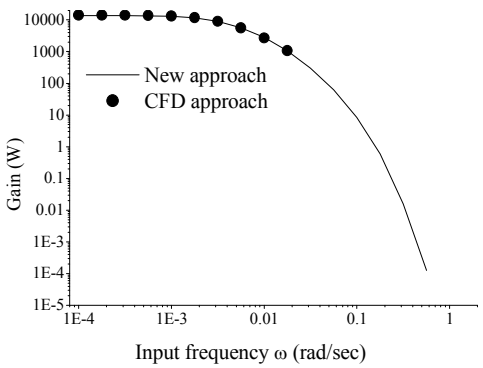

Fig. 6 Comparison of the gain with dynamic temperature $\tilde{\theta} = 110 * \sin(\omega t)\ K$ on BC1

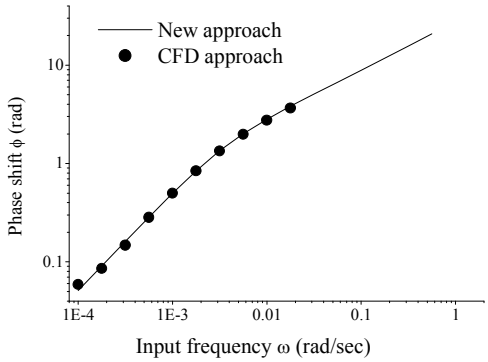

Fig. 7 Comparison of the phase shift with dynamic temperature $\tilde{\theta} = 110 * \sin(\omega t)\ K$ on BC1

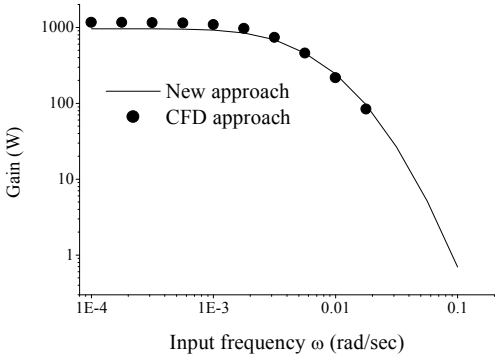

Fig. 8 Comparison of the gain with dynamic heat flux $\tilde{Q}_{BC2} = -2 * 10^4\ sin(\omega t)\ W/m^2$ on BC2

The comparison of the frequency responses obtained by the proposed approach and CFD approach is given in Figs. 6 and 7. It can be seen that the agreement between the two is excellent. However, the proposed method has an advantage at higher frequency, as it does not suffer from numerical errors. Figures 8 and 9 show the gain and phase shift on the boundary BC4 when the dynamic heat flux is applied on BC2. Figures 10 to 13 show the comparison of the

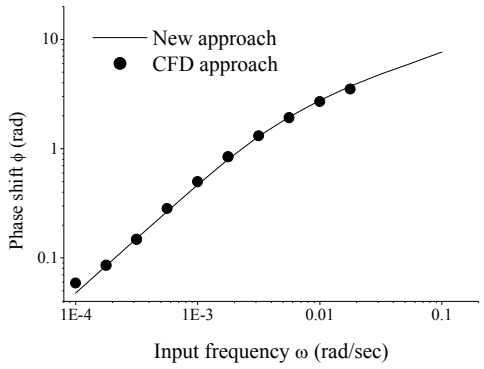

Fig. 9 Comparison of phase shift with dynamic heat flux $\widetilde{Q}_{BC2} = -2*10^4\ sin(\omega t)\ W/m^2$ on BC2

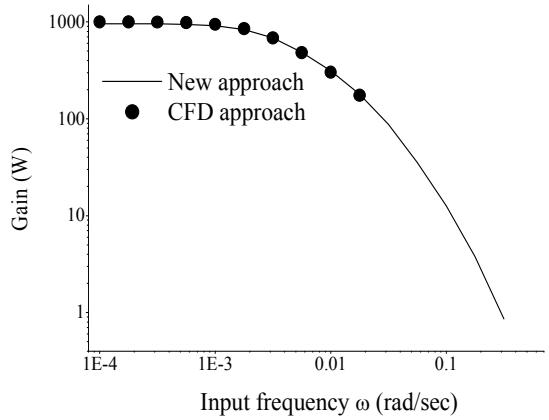

Fig. 10 Comparison of gain with the dynamic heat transfer coefficient $\widetilde{h}_{BC3} = 20\,sin(\omega t)\ W/m^2 \cdot K$ on BC3

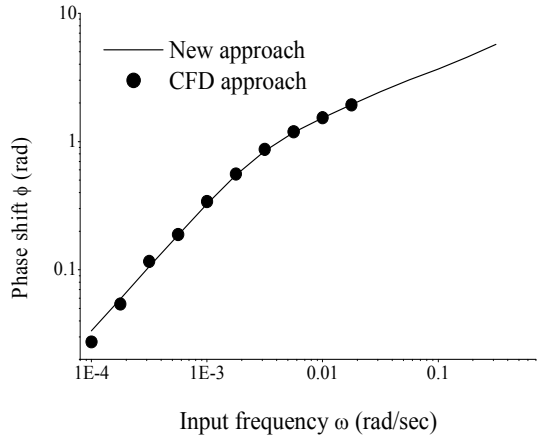

Fig. 11 Comparison of the phase shift with the dynamic heat transfer coefficient $\widetilde{h}_{BC3} = 20\,sin(\omega t)\ W/m^2 \cdot K$ on BC3

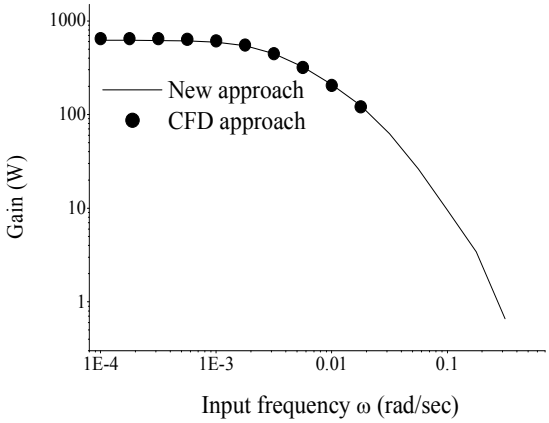

Fig. 12 Comparison of the gain with the dynamic ambient temperature $\widetilde{\theta}_{\infty,BC3} = 25\,sin(\omega t)\ K$ on BC3

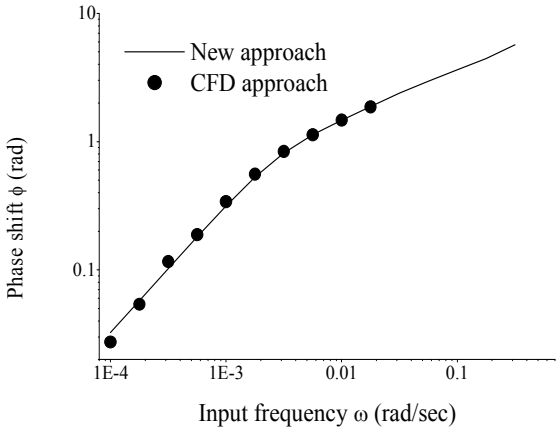

Fig. 13 Comparison of the phase shift with the dynamic ambient temperature $\widetilde{\theta}_{\infty,BC3} = 25\,sin(\omega t)\ K$ on BC3

frequency responses when the dynamic heat transfer coefficient and ambient temperature (convective heat transfer boundary condition) is applied on BC3. It can be concluded that the agreement between the frequency responses using both approaches is excellent under all three types of dynamic boundary conditions.

4 Conclusions

In this paper, a new approach is proposed to solve the 2D heat transfer problem in the frequency domain with a nonlinear source term. The expressions of three types of heat transfer boundary conditions in the frequency domain are derived. The performance of the proposed approach has been validated against the results obtained from full-scale CFD simulation and excellent agreement has been obtained. The

comparison between the results from the proposed approach and the CFD approach indicates that the proposed approach can produce almost the same results as CFD approach in low to medium frequency range, but in high frequency range, the proposed scheme outperforms the CFD approach. Furthermore, once the heat transfer problem is captured in terms of transfer functions, it practically takes no time to obtain the system response. This approach is suitable for heat transfer problems with nonlinear source terms under all three types of heat transfer boundary conditions.

References

[1] Nyquist, H., Regeneration Theory, *Bell Systems Technical Journal*, 11:126-147 (1932).

[2] Lu, Q., Sun, Y. and Mei, S., *Nonlinear Control Systems and Power System Dynamics*, Kluwer Academic Publishers, Norwell, Massachusetts, 2001.

[3] Nise, N. S., *Control System Engineering*, John Willy & Sons Inc., New York, 2000.

[4] Bohn, D., Deutsch, G. and Krueger, U., Numerical Prediction of the Dynamic Behavior of Turbulent Diffusion Flames, *Journal of Engineering for Gas Turbines and Power,* 120(4):713-720 (1998).

[5] Polifke, W., Poncet, A., Paschereit, C. O. and Dobbeling, K., Reconstruction of Acoustic Transfer Matrices by Instationary Computational Fluid Dynamics, *Journal of Sound and Vibration*, 245(3):483-510 (2001).

[6] Jiang, Q., Zhang, C. and Jiang, J., An Industrial Reheating Furnace with Flue Gas Recirculation Modeled by Linear Transfer Functions, *Combustion Science and Technology*, 176:1473-1464 (2004).

[7] Jiang, Q., Zhang, C. and Jiang, J., Sensitivity Analysis of a FGR Industrial Furnace for NOx Emission Using Frequency Domain Method, *ASME Trans. Journal of Energy Resources Technology* (accepted, 10/21/05).

[8] Zhang R., Zhang C. and Jiang J., A New Approach for Direct Solution of 2D Heat Transfer Problem with Nonlinear Source Terms in Frequency Domain, *International Journal of Nonlinear Sciences and Numerical Simulation*, 7(3): 295-298 (2006).

[9] Patankar, S.V., *Numerical Heat Transfer and Fluid Flow*, Hemisphere, New York, 1980.